photonics

MDPI

Article

Design and Numerical Analysis of an Ultra-Sensitive π-Configuration Fibre Optic-Based SPR Sensor: Dual Plasmonic Enhancement for Low-Refractive-Index Biomolecular Detection

John Ehiabhili, Radhakrishna Prabhu * and Somasundar Kannan

School of Computing and Engineering Technology, Robert Gordon University, Aberdeen AB10 7GJ, UK; j.ehiabhili@rgu.ac.uk (J.E.); s.kannan1@rgu.ac.uk (S.K.)
* Correspondence: r.prabhu@rgu.ac.uk

Abstract

Surface plasmon resonance (SPR)-based optical fibre sensors have transformed label-free biosensing; however, single-interface evanescent field interactions continue to limit their sensitivity. This study presents a novel π-configuration optical fibre-based surface plasmon resonance sensor that greatly increases sensitivity by enabling dual plasmonic excitation on two symmetrically polished surfaces coated with optimized metallic thin films (Ag, Au, or Cu). We show, using finite element method simulations in COMSOL Multiphysics v6.3, that the π-configuration increases the interaction volume between the analyte and guided light, resulting in an enhanced sensitivity of 3300 nm/RIU for silver at refractive index (RI) 1.37–1.38, which is a 120% improvement over traditional D-shaped sensors (1500 nm/RIU). The maximum field norm for the π-configuration sensor is approximately 1.4 times greater than the maximum observed for the D-shaped SPR sensor at an analyte RI of 1.38. The sensor's performance is evaluated using full-width half-maximum, wavelength sensitivity, and wavelength interrogation metrics. For the π-configuration sensor at an analyte RI of 1.38, the values of the FWHM, figure of merit, detection accuracy, and confinement loss were 36 nm, 94.29 RIU^{-1}, 0.94, and 38.5 dB/cm, respectively. The results obtained are purely simulated using COMSOL. With the support of electric field confinement analysis, a thorough theoretical framework describes the crucial coupling regime that causes ultra-high sensitivity at low RI. This design provides new opportunities for environmental monitoring, low-abundance biomarker screening, and early-stage virus detection, where it is necessary to resolve minute RI changes with high precision.

Keywords: SPR; D-shaped optical fibre; π-configuration; dual plasmonic coupling; finite element method (FEM); biosensing

Check for updates

Received: 20 August 2025
Revised: 16 January 2026
Accepted: 30 January 2026
Published: 3 February 2026

Copyright: © 2026 by the authors. Licensee MDPI, Basel, Switzerland. This article is an open access article distributed under the terms and conditions of the Creative Commons Attribution (CC BY) license.

1. Introduction

The use of optical fibre sensors based on surface plasmon resonance (SPR) has revolutionized label-free biosensing by providing high-sensitivity, real-time biomolecular interaction detection [1]. Surface plasmon resonance (SPR) is a quantum optical phenomenon caused by the coherent oscillation of free electrons at the interface of a metal and a dielectric when excited by incident light. These resonant oscillations, known as surface plasmon polaritons (SPPs), are transverse magnetic (TM) polarized electromagnetic waves that propagate along the interface before decaying evanescently into both media. SPP excitation requires both energy and momentum conservation, which is normally met at a

specific wavelength or angle of incidence. This resonance is seen as a sharp attenuation in the reflected or transmitted light spectrum. The resonant condition is highly sensitive to changes in the local refractive index within the evanescent field's penetration depth. Any change shifts the phase-matching requirement, affecting the resonance position. This fundamental sensitivity serves as the physical foundation for SPR-based sensing, which allows for the direct detection of molecular interactions and biochemical analytes without the use of labels [2,3]. Clinical diagnostics and drug discovery have made extensive use of traditional SPR systems, such as prism-coupled Kretschmann and Otto configurations [4]. However, because of their bulkiness and alignment sensitivity, miniaturized fibre-optic alternatives have been developed [5]. D-shaped SPR sensors are at the forefront of this movement because of their increased evanescent field interaction, compact form factor, and remote sensing capabilities [6]. To produce controlled evanescent field interaction while preserving structural integrity, researchers carefully polished one side of the fibre to reveal the core and then deposited a thin metal film [7,8]. Later studies have concentrated on improving the many aspects of D-shaped SPR sensors, such as the metal film properties, polishing depth, and interrogation techniques [9,10]. By showing that the best sensitivity occurs when the metal layer thickness is maintained between 40 and 50 nm and the residual cladding thickness is decreased to roughly 0.5–1 μm, Homola and colleagues' work revealed crucial design principles [11]. While reducing optical losses, these parameters provide an adequate evanescent field strength at the metal–dielectric interface [12]. Despite these benefits, fundamental restrictions in plasmonic field confinement and interaction volume still limit the sensitivity of single-interface D-shaped sensors, especially for low-concentration analytes where minute RI changes (~10^{-4}–10^{-5} RIU) need to be resolved [13].

In the development of SPR sensors, material selection for the plasmonic layer has also been the subject of extensive research [14]. Due to its well-characterized optical characteristics and chemical stability, gold has long been the standard; yet, its ultimate sensitivity is limited by rather large optical losses in specific wavelength ranges [15]. Although silver has a stronger field enhancement and smaller losses than other metals, its practical use has historically been limited due to its oxidation tendency [16]. The use of ultrathin alumina or graphene layers, among other recent developments in protective coating technologies, has reignited interest in silver-based SPR sensors [17]. Although copper performs less than both gold and silver, it has also been investigated as a less expensive option [18]. Sensor performance across a range of wavelengths is greatly influenced by these metals' dielectric characteristics, especially their frequency-dependent permittivity as defined by the Drude–Lorentz model [19].

To balance sensitivity and signal-to-noise ratio, recent developments in D-shaped SPR sensors have concentrated on improving geometric parameters, such as metal film thickness (40–50 nm) and width (10 μm), as well as material selection (Ag, Au, and Cu). Due to its strong plasmonic response and low optical losses, as measured by the ratio of the real to imaginary parts of its dielectric function (n/κ), silver has shown excellent performance in the visible-to-near-infrared (NIR) range [20]. Even the most advanced single-polished D-shaped devices, however, are unable to provide the sensitivity needed for new applications where analyte concentrations frequently dip below picomolar levels, including low-abundance biomarker screening or early-stage virus detection. This constraint is caused by the single-sided interaction geometry and the limiting evanescent field penetration depth, which inherently limit the sensor's capacity to amplify minute RI fluctuations [21].

To address these challenges, we propose a novel pi (π)-configuration fibre optic-based SPR sensor. The π-configuration sensor is created by side-polishing two opposite sides of a single-mode optical fibre. The cladding is partly removed, creating a geometry that resembles the Greek letter "Π" (pi), where the two vertical legs represent the two polished

regions, and the horizontal bar represents the remaining cylindrical cladding and core region in the centre. The π-configuration geometry is a symmetrically layered, dual-channel SPR sensor whose novelty lies in the specific optical and plasmonic interactions this symmetry enables. By permitting simultaneous SPP excitation at both metal–dielectric boundaries, this dual-interface design essentially redefines the dynamics of the sensor's interaction and increases the overlap of the evanescent field with the analyte. By utilizing constructive interference between the two plasmonic zones, the π-configuration produces a synergistic sensitivity boost that is especially noticeable in the low-RI range (1.37–1.38), where traditional sensors show declining returns. According to theoretical models, this geometry functions close to a critical coupling situation, where the combined effects of improved field confinement and mode hybridization cause minor RI perturbations to produce disproportionately large resonance wavelength shifts [22].

These predictions are supported by finite element method (FEM) simulations in COMSOL Multiphysics v6.3, which show that the π-configuration has a remarkable sensitivity of 3300 nm/RIU for silver at RI 1.37–1.38, which is 120% better than the single D-shaped design (1500 nm/RIU). Silver's special plasmonic characteristics, such as its low damping coefficient (γ) and strong negative real permittivity ($\varepsilon_m{}'$), are responsible for this nonlinear response. These characteristics maximize field enhancement at the dual interfaces while minimizing optical losses [23]. However, because of their larger intrinsic losses and inter-band transitions, gold and copper show more moderate benefits in the π-configuration, highlighting the material-specific character of this enhancement [24]. The sensor's superiority for low-RI biosensing applications is confirmed by rigorous metrics including amplitude sensitivity, full-width half-maximum (FWHM), and detection accuracy (DA), which further quantify its performance.

This work has far-reaching consequences that go well beyond incremental sensitivity improvements. The dual-plasmonic architecture of the π-configuration sensor fills a crucial gap in the detection of diluted analytes, including viruses, exosomes, and environmental pollutants, where conventional SPR systems fall short. Its seamless integration into lab-on-a-chip and point-of-care platforms is ensured by its compatibility with current fibre-optic fabrication procedures, such as side-polishing and magnetron sputtering [25]. In addition to expanding our basic knowledge of multi-interface plasmonic coupling, our work opens the door for next-generation biosensors that can function at the cutting edge of molecular detection. To fully realize the potential of this revolutionary technology, future research will investigate multiplexed detection approaches, biofunctionalization techniques, and experimental validation.

2. Theoretical Design and Numerical Modelling

The novel dual-plasmonic excitation architecture of the π-configuration optical fibre-based SPR sensor marks a significant departure from conventional single-interface devices. This sensor's theoretical framework introduces new considerations for coupled-interface phenomena while expanding upon basic SPP propagation principles. The proposed π-configuration sensor is fabricated by precisely polishing a typical SMF with a germanium-doped silica core and pure silica cladding to generate two opposing, parallel flat surfaces. The core is brought to 700 nm away from each surface to provide robust evanescent field access. This important phase can be accomplished with a V-groove polishing jig that ensures parallelism and precise control over the residual cladding thickness [26]. Photolithography defines the key π-configuration structure. A layer of positive photoresist is spun onto the sample and soft-baked. The sample is then subjected to UV light via a photomask, resulting in two parallel sensing layer patterns on either side of the fibre [27]. After development, the sensing region pattern is transferred to the photoresist, leaving the fibre cladding

exposed in the areas where metal will be deposited via thermal evaporation or magnetron sputtering techniques [28]. A thin adhesion layer, such as titanium, is deposited via electron beam evaporation, followed by a 45 nm layer of metal (Ag or Au) with a precise 10 μm width, which functions as both the sensing and plasmonic layers. The lift-off operation, which involves immersing the sample in a resist remover solvent, removes surplus metal from the photoresist, revealing clean, well-defined parallel metal sensing layers of the π-configuration on the fibre cladding.

With the help of this symmetric arrangement, counter-propagating SPP modes can be excited simultaneously and interact coherently with the guided core mode to create an interference pattern that increases sensitivity to changes in the refractive index [29]. The π-configuration optical fibre-based SPR sensor's 3D schematics are displayed in Figure 1a, and its 2D cross-section is displayed in Figure 1b.

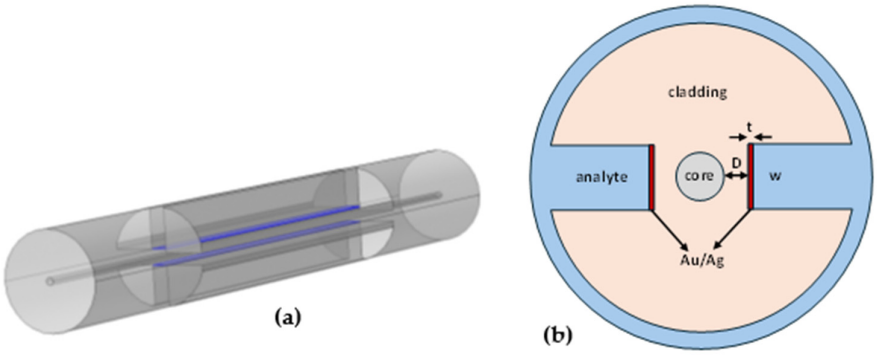


Figure 1. (**a**) The 3D schematic of π-config D-SPR sensor; (**b**) sensor design in 2D with core design parameters (residual cladding thickness D = 700 nm, the metal film width w = 10 μm, and the metal film thickness t = 45 nm).

The proposed sensor's operational principle is determined by the interaction of waveguide optics and electro-optics. The COMSOL Wave Optics Module used a Port boundary condition to excite the fibre's fundamental eigenmode (HE_{11}). To assess the sensor's spectral response, the source was defined as a forward-propagating light wave with a wavelength parametrically swept across the visible to near-infrared spectrum (600 nm to 1200 nm). This frequency-domain study provided steady-state field distributions and transmission data at each discrete wavelength, allowing for a thorough analysis of spectral performance. Light is confined within the optical fibre core through total internal reflection (TIR). This occurs when light propagating in the core strikes the interface, the cladding, at an angle greater than the critical angle [30]. The solution of Maxwell's equations under these boundary conditions generates guided modes, each with a separate propagation constant, β. The HE_{11} mode used in this study has an evanescent field that extends a fraction of a wavelength into the cladding. It serves as a vital probe for external perturbations, as it is sensitive to changes in the surrounding dielectric environment.

The π-configuration sensor's electromagnetic behaviour is controlled by altered phase-matching requirements that take dual-interface coupling into consideration. To incorporate contributions from both metal–dielectric interfaces, the conventional SPR condition, which is written as $\mathrm{Re}(\beta_{SPP}) = \mathrm{Re}(\beta_{guided})$, where β_{SPP} and β_{guided} stand for the propagation constants of the surface plasmon and guided modes, respectively, must be extended [31]. This results in a set of interconnected equations that characterize the hybridized plasmonic modes:

$$\beta_{eff} = \beta_{guided} + \Delta\beta_1 + \Delta\beta_2 \quad (1)$$

where $\Delta\beta_1$ and $\Delta\beta_2$ represents the disruption to the propagation constant that each plasmonic contact induces. The Drude–Lorentz model is used to represent the frequency-

dependent dielectric function of the metal, $\varepsilon_{m(\omega)}$, adding interband transition and free-electron contributions [32]:

$$\varepsilon_m(\omega) = \varepsilon_\alpha - \frac{\omega_P^2}{\omega^2 + i\gamma\omega} + \Delta\varepsilon_P \frac{\Omega_P^2}{\Omega_P^2 - \omega^2 - i\Gamma_P\omega} \quad (2)$$

where ω_p is the plasma frequency, γ is the damping coefficient, and the summation accounts for Lorentz oscillator terms representing interband transitions. For silver and gold, these values are obtained from the literature [20] and yield excellent agreement with experimental data across the visible to near-infrared spectrum.

COMSOL Multiphysics v6.1 with the Wave Optics Module was used to numerically analyze the π-configuration sensor. A full-vectorial finite element method (FEM) technique was used to solve Maxwell's equations in three dimensions. The analysis involves the propagation of light in the optical fibre (wave optics). The propagation of light in the optical fibre was modelled using the wave equation, derived from Maxwell's equations. For a time-harmonic field, the equation for the electric field $\vec{E}_0$ is [33]:

$$\nabla \times \left(\nabla \times \vec{E}_0 \right) - k_0^2 \varepsilon_r \vec{E}_0 = 0 \quad (3)$$

where $k_0 = \omega\sqrt{\mu_0\varepsilon_0}$ is the wave number in free space, ε_0 is the permittivity of free space, μ_0 is the permeability of free space, ε_r is the relative permittivity (dielectric constant) of the material and ω is the angular frequency. In our 2D models, this equation was solved as an eigenfrequency problem to find the supported modes and their effective indices, n_{eff}.

A 125 μm diameter fibre segment with two sharply contrasted polished regions, each with a 10 μm wide metal coating, was part of the computational domain. While a scattering boundary condition managed outgoing radiation, a perfectly matched layer (PML) boundary condition with a quadratic absorption profile was used to reduce spurious reflections. A port boundary condition with incident power normalization of 1 W was applied at the input, and the transmitted power and mode overlap were determined at the output using a matched port. The continuity condition was applied to all interior interfaces, including the core-cladding boundary and the dielectric–metal interfaces, to ensure proper physical behaviour of tangential field components. The sensing layers in the π-configuration were explicitly modelled as lossy metal thin-films using a Transition Boundary Condition (TBC), which accurately reflects the finite conductivity and field penetration effects necessary for a realistic performance assessment. A physics-controlled very-fine triangular mesh was used to precisely optimize the mesh, guaranteeing numerical accuracy while preserving computational performance. With the surrounding analyte medium modelled as a homogeneous dielectric with a tuneable refractive index, material dispersion was integrated using Sellmeier equations for silica and experimental data for metal dielectric functions. The Sellmeier equation is used to calculate the RI of the silica cladding and the Ge doped core [34]:

$$n^2(\lambda) = 1 + \frac{B_1\lambda^2}{\lambda^2 - C_1} + \frac{B_2\lambda^2}{\lambda^2 - C_2} + \frac{B_3\lambda^2}{\lambda^2 - C_3} \quad (4)$$

where B_1, B_2, B_3, C_1, C_2, and C_3 are Sellmeier's constants, n is the optical fibre core or cladding wavelength-dependent RI, and λ is the incident light wavelength in microns.

A modal research study was conducted to determine the complex effective indices ($n_{eff} = n_{real} + n_{imag}$) of supported modes in the 600–1200 nm wavelength range. This was followed by a frequency-domain investigation to calculate transmission spectra and field distributions. A crucial indicator of SPR sensor performance, confinement loss,

was computed using the imaginary portion of the effective refractive index from the expression [35]:

$$L_c = 8.686 \times \left(\frac{2\pi}{\lambda}\right) \times \left(n_{eff}\right)_{imag} [\mathrm{dB/m}] \quad (5)$$

At the metal–dielectric interfaces, energy is transferred from the guided core mode to the plasmonic modes, resulting in this loss process. The fundamental mode was propagated via a sensing region that was 500 mm long. The output power normalized to input was then calculated to give the transmission coefficient $T(\lambda)$ expressed as [36] follows:

$$T(\lambda) = \exp\left(\frac{4\pi}{\lambda}.\left(n_{eff}\right)_{imag}.L\right) \quad (6)$$

where L is the length of the sensing region. The sensitivity, S of a sensor is the ratio of the change in output signal (resonant wavelength) to the corresponding change in input signal (analyte RI) [37]. Resonance wavelengths were identified as minima in the transmission spectrum, with sensitivity, S, calculated from the spectral shift $\Delta\lambda_{res}$ per analyte refractive index unit (RIU) change Δn_a.

$$S\ (nmRIU^{-1}) = \frac{\Delta\lambda_{res}}{\Delta n_a} \quad (7)$$

The resolution, R, of a sensor is a measure of the smallest detectable change in the analyte RI or concentration. A dimensionless quantity that combines the FWHM and sensitivity to evaluate the sensor's performance is the figure of merit (FOM). The full width at half maximum (FWHM) of the spectra is a measure of the sharpness of the resonance [38].

$$R = \frac{\Delta\lambda_{min}}{S} \quad (8)$$

$$FOM = \frac{S}{FWHM} \quad (9)$$

A sensor's coupling efficiency $\eta(\lambda)$ refers to how much incident light in the optical fibre effectively couples into the surface plasmon mode at the metal–dielectric interface. It is a determining factor in the sharpness of the resonance peak and the sensor's sensitivity [39]. It is usually expressed as a percentage and is given as

$$\eta(\lambda) = 1 - T(\lambda) \quad (10)$$

The field penetration depth, d_p is the depth from the metal–dielectric interface into the dielectric at which the amplitude of the electric field decays to $1/e$ of its value at the interface. This exponential decay is because of the electromagnetic wave interacting with the electrons in the metal [40]. This is expressed as

$$d_p = \frac{\lambda}{2\pi}\left[\frac{|\,\varepsilon_m + \varepsilon_d\,|}{\varepsilon_d^2}\right]^{1/2} \quad (11)$$

where ε_m is the complex permittivity of the metal, ε_d is the permittivity of the dielectric, and λ is the wavelength of incident light.

Convergence testing and comparison with published single-interface D-shaped sensor data were used to validate the numerical model [20]. By gradually increasing the element size until variances in the calculated effective index dropped below 0.1%, mesh independence was verified. Additional confirmation of the expected dual-interface coupling behaviour was carried out for the π-configuration by analyzing field distributions.

With distinctive exponential decay into the analyte and fibre core areas, the electric field profiles amply demonstrated symmetric enhancement at both metal–dielectric interfaces. The operating principle of the dual-coupled design was confirmed by power flow analysis, which showed the anticipated energy transfer from the core mode to plasmonic interfaces. These thorough numerical investigations offer a solid theoretical basis for the remarkable sensitivity improvement seen in the π-configuration sensor.

3. Results and Discussion

3.1. Wavelength Sensitivity Analysis

When compared to conventional single-interface D-shaped sensor designs, the π-configuration SPR sensor's spectral response demonstrated a notable improvement in wavelength sensitivity. The π-configuration showed an exceptional sensitivity of 3300 nm/RIU for silver-coated sensors that analyzed RI changes from 1.37 to 1.38. This is a 120% improvement over the 1500 nm/RIU attained by the D-shaped equivalent. At higher refractive index changes, this nonlinear amplification decreased; when detecting changes from 1.38 to 1.39, the π-configuration showed 4400 nm/RIU versus 4200 nm/RIU for the D-shaped design. The π-configuration's distinct field distribution shifts the operating resonance wavelength for a given analyte RI, resulting in a significant 120% enhancement for silver in the 1.37–1.38 RIU range. Silver's complex permittivity ($\varepsilon(\omega) = \varepsilon' + \varepsilon''$) is strongly dependent on wavelength. This resonance condition in the lower RI range overlaps with a spectral region where the real part of the permittivity (ε') is more negative and material loss (controlled by ε'') is minimal [41]. This results in a sharp and high-quality-factor plasmon resonance. The π-configuration sensing layers' strong, symmetric field confinement enhances the ideal resonance, resulting in a significantly greater differential wavelength shift, $\frac{d\lambda}{dn}$, compared to the D-shaped design for that incremental RI change. In the 1.38–1.39 RIU range, both sensors' resonance wavelengths change to a spectral region with high optical losses in silver (ε'' becomes bigger). In this lossier regime, the benefit of the π-configuration's field structure fades, as the plasmon resonance broadens for both sensor types. As a result, their diverse sensitivities converge. This metal-specific, resonance-dependent performance highlights that the enhancement factor is not a universal constant but a function of the operating point relative to the material's dispersion. The π-configuration offers the greatest advantage when it enables operation at a metal's "hot-spot" for plasmonic excitation. Similar patterns were seen in the implementations of copper and gold, although the enhancement was less noticeable. For analyte RI change from 1.37 to 1.38, gold showed 3300 nm/RIU (π-configuration) versus 3200 nm/RIU (D-shaped), and for 1.38–1.39, 4300 nm/RIU compared to 4200 nm/RIU. With an increasing refractive index, the sensitivity curves as functions of wavelength showed a characteristic red shifting of resonance dips. The π-configuration showed a wider dynamic range and more pronounced dip formation, especially in the 650–850 nm spectral region where silver's plasmonic response is most efficient.

The transmission spectra for D-shaped SPR sensor and the π-configuration SPR sensor configuration using silver metal thin-film were obtained for analyte refractive indices varying from 1.37 to 1.42 and are shown in Figures 2a and 2b, respectively.

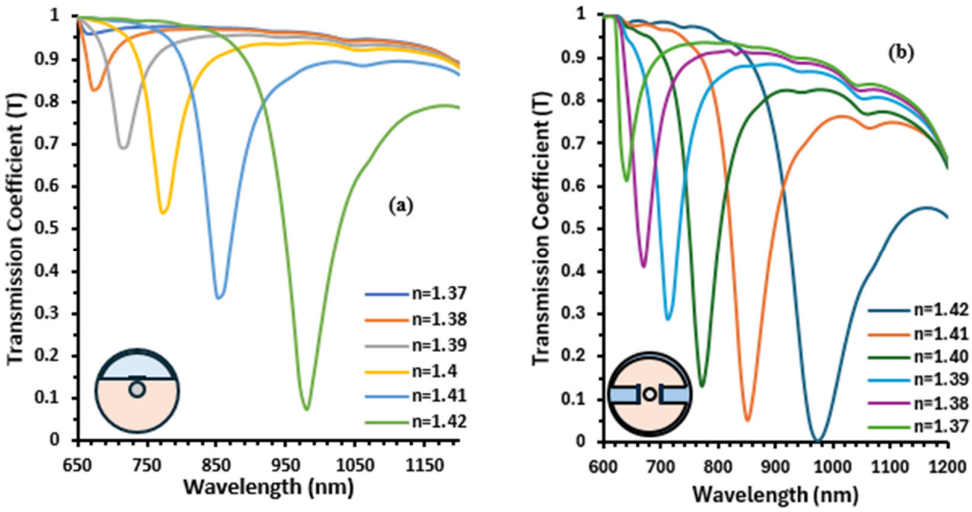


Figure 2. Transmission spectrum for (**a**) D-shaped SPR sensor; (**b**) π-shaped SPR sensor.

The inset in each figure shows a 2D schematic of the SPR sensors. The wavelength of light was varied from 600 to 1200 nm, covering part of the visible and near-infrared region. Since the same metal thin film was used for each of the sensing surfaces for the π-configuration SPR sensor configuration, only one distinct resonance dip corresponding to the plasmonic interactions of the metals with the analyte was observed. The π-configuration dual-interface design enhances interaction between the guided mode and the surface plasmons, leading to sharper resonance dips for small RI changes. To quantitatively compare the performance improvement offered by the π-configuration relative to the conventional D-shaped design, an enhancement factor (*EF*) was calculated for each performance metric. The enhancement factor for sensitivity, EF_S, is defined as the ratio of the sensitivity of the π-configuration sensor, S_π, to the sensitivity of the D-shaped sensor, S_D, for the same range of analyte refractive index change:

$$EF_S = \frac{S_\pi}{S_D} \tag{12}$$

An $EF_S > 1$ indicates a performance enhancement by the π-configuration, with the value quantifying the factor of improvement. This same ratio-based methodology was applied to calculate enhancement factors for other metrics, such as the electric field vector, FWHM, detection accuracy, FOM, penetration depth, and coupling efficiency.

Through rigorous numerical simulations, the spectrum performance characteristics of both traditional D-shaped SPR sensors and those with a π-configuration were quantitatively assessed. The comparative wavelength sensitivity statistics for various metal coatings and RI ranges are shown in Table 1. Silver performs exceptionally well in the π-configuration, according to the data, especially at lower refractive indices where the dual-interface coupling effect is most noticeable. With a nonlinear trend, the sensitivity enhancement converges with conventional D-shaped designs at higher indices after reaching its maximum significance in the 1.37–1.38 RI range.

Table 1. Comparison of wavelength sensitivity and enhancement.

Metal Thin Film	RI Range	π-Configuration Sensitivity (nmRIU^{-1})	D-Shaped Sensitivity (nmRIU^{-1})	Enhancement Factor
Ag	1.37–1.38	3300	1500	2.20×
	1.38–1.39	4400	4200	1.05×
Au	1.37–1.38	3300	3200	1.03×
	1.38–1.39	4300	4200	1.02×
Cu	1.37–1.38	3100	2900	1.07×
	1.38–1.39	4100	4000	1.03×

The observed sharp enhancement peak and subsequent drop in performance are quantitatively explained through effective index analysis. Figure 3 reveals that in the 1.37–1.38 refractive index window, the real effective index of the π-configuration's core mode $Re(n_{eff}) = 1.4567$ and $Re(n_{eff}) = 1.4561$, respectively, converges with the real part of the SPP effective index $Re(n_{SPP})$, satisfying the resonant phase-matching condition $Re(n_{eff}) = Re(n_{SPP})$ for optimal excitation. This precise alignment maximizes the evanescent field coupling and yields the peak enhancement factor of 2.20×. For analyte indices beyond 1.38, the SPP dispersion curve steepens considerably, outpacing the shift in the core mode's effective index. This divergence introduces a significant phase mismatch, disrupting resonant coupling and causing the enhancement to fall to 1.05×.

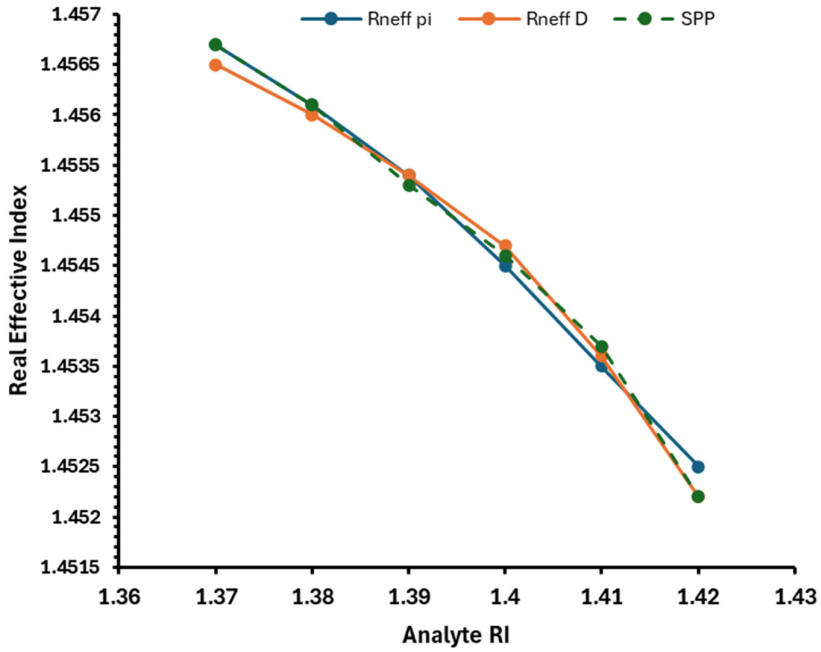


Figure 3. Phase matching plot showing $Re(n_{SPP})$ and $Re(n_{eff})$ for D-shaped and π-shaped SPR sensors.

Beyond simple phase-matching, the π-geometry relies on constructive interference between counter-propagating SPP modes. While a marginal effective index mismatch persists at $n_a = 1.39$, the more critical factor is the alteration in the SPP propagation length L_{SPP}, which is highly sensitive to the imaginary part of the metal's dielectric function, $Im(\varepsilon_{Ag})$. In the optimal 1.37–1.38 range, L_{SPP} is tuned to satisfy the π-phase accumulation condition over the sensing length. A slight increase in analyte index perturbs $Im(n_{SPP})$,

reducing L_{SPP} and degrading the interferometric enhancement that defines the π-sensor's superior performance. Thus, the narrow operational window is not a drawback but a direct manifestation of the sensor's heightened selectivity, making it exceptionally suitable for detecting subtle refractive index changes within a precisely defined background medium.

The dispersion curves in Figure 4 provide quantitative evidence of the enhanced coupling mechanism in the π-configuration. It shows a plot of the $Re\left(n_{eff}\right)$ against wavelength for the core, D-shaped SPP, and π-configuration SPP modes. At the analyte refractive index of 1.38, the π SPP mode intersects the core (HE_{11}) mode precisely at its resonance wavelength of 669 nm, fulfilling the condition $Re(n_{SPP}) = n_{core}$ required for optimal phase-matching and critical coupling (orange dot in the inset). In contrast, the single-interface SPP mode of the D-shaped sensor does not intersect the core mode at its resonance peak (674 nm), confirming its suboptimal coupling, as seen by the blue dot in the inset of the figure. This exact spectral alignment in the π-sensor creates a steeper effective-index slope ($\frac{dn_{eff}}{d\lambda}$), which directly translates into the observed large wavelength shift and heightened sensitivity, confirming that the performance enhancement stems from a tuned hybridization and critical coupling condition.

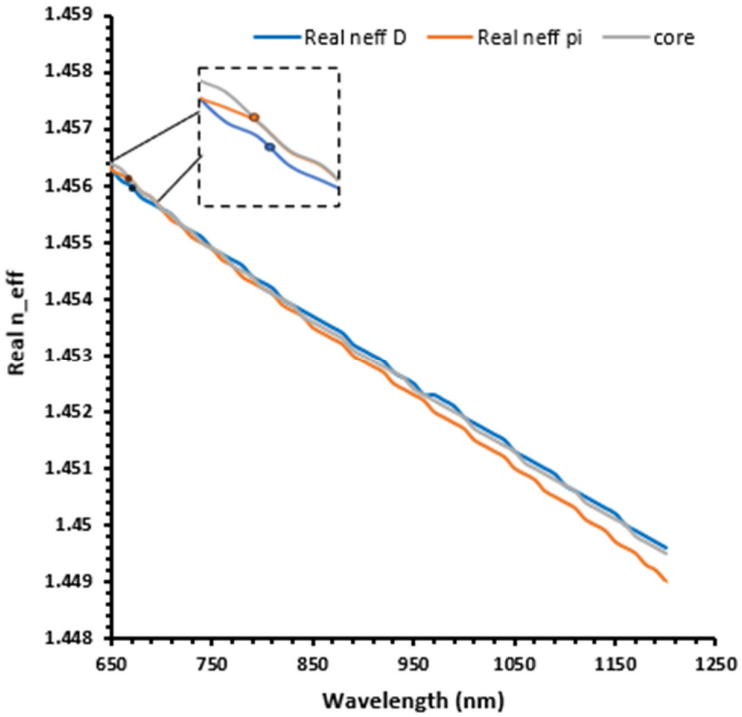


Figure 4. Dispersion relations for the core (HE_{11}) mode, D-shaped SPP mode, and π-hybridized SPP mode at RI = 1.38.

3.2. Electric Field Confinement and Enhancement

The π-configuration and conventional D-shaped sensors showed significant variances in field distribution, according to full-wave electromagnetic simulations. With peak field intensities almost 1.4 times higher than those seen in single-interface designs, the dual-interface design generated symmetric electric field augmentation at both metal–dielectric interfaces. The expected exponential decay profile was followed by the field penetration depth into the analyte medium; however, the opposing evanescent fields from both interfaces resulted in a slightly prolonged interaction volume. Particularly at resonance wavelengths, the constructive interference patterns between the two plasmonic zones were evident in the $|E|^2$ field maps, resulting in localized "hot spots" of increased electromagnetic energy density. Figure 5 shows the simulated electric field intensity distribution at

the metal–dielectric interfaces of the SPR optical fibre sensors for the (a) D-shaped and the (b) π-configuration. These images provide an impression of the localization and intensity of the plasmonic excitation, confirming the phase-matching conditions of the SPR modes. The π-configuration benefits from a symmetric and direct field path between two closely spaced, parallel sensing regions. This geometry efficiently concentrates the field lines within the fibre structure, leading to a higher peak field intensity. In the D-shaped configuration, the sensing region on a single plane adjacent to the fibre core creates a highly localized but less intense field. The field fringes significantly into the surrounding low-permittivity medium, reducing the overall field concentration within the fibre itself compared to the confined, cladding-filled path in the π-configuration.

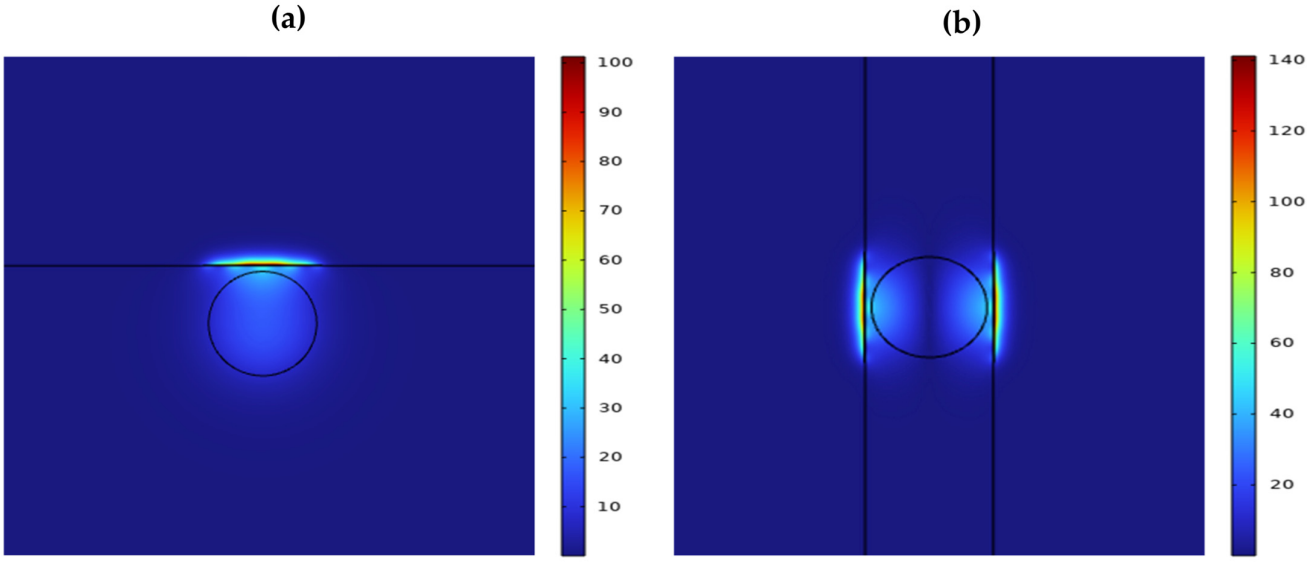


Figure 5. Electric field distribution for (**a**) D-shaped SPR mode; (**b**) π-config SPR mode.

Using similar metal thin-films in a dual-sensing-region π-configuration arrangement advances the field of SPR-based fibre optic sensing and has the unique benefit of separating the geometric contribution to crosstalk (opposite-side polishing) from material effects. This offers a baseline for the many hybrid arrangements as sensing regions.

The electric field norm $|E|$ is a crucial parameter for understanding a sensor's behaviour especially in relation to its spatial resolution and sensitivity. The arc length is the distance from the sensor's surface into the dielectric (analyte or surrounding medium). Figure 6a,b shows the graph of the sensors electric field norm against the arc length for the π-configuration and the D-shaped SPR-based fibre sensors, respectively. The maximum field norm for the π-configuration sensor is approximately 140 V/m at an analyte RI of 1.38, which is 1.4 times greater than the maximum observed for the D-shaped SPR sensor. The higher magnitude in electric field at the peak indicates a higher response to changes in that precise location, eventually leading to a localized region of high sensitivity, which is ideal for applications where a high spatial resolution is needed to detect an event at that location.

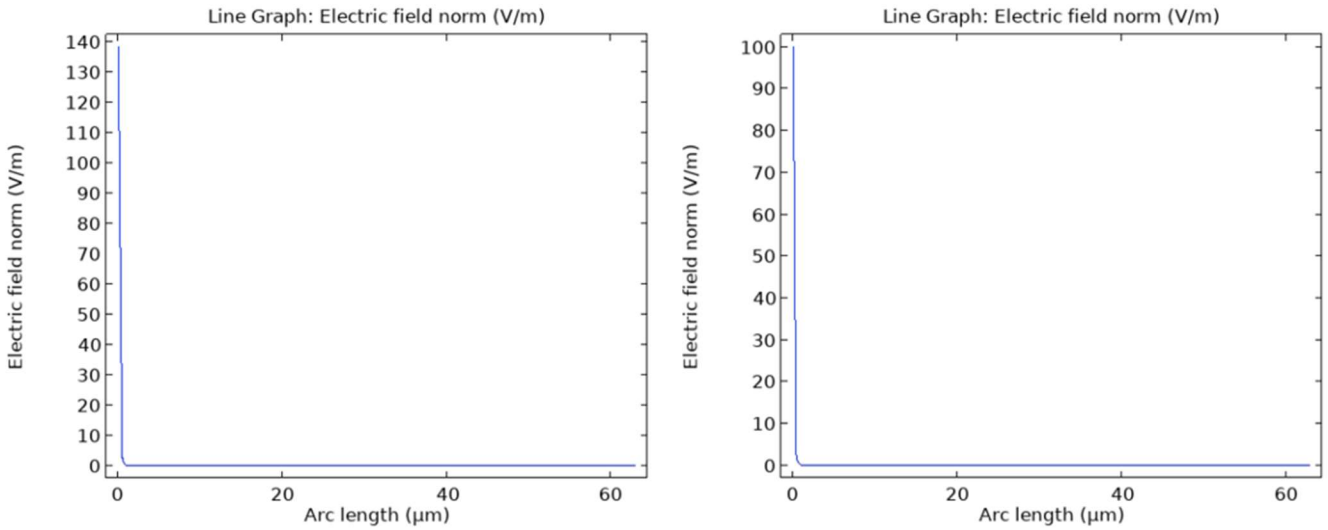


Figure 6. Graph of electric field norm vs. arc length for (**a**) π-configuration; (**b**) D-shaped sensor.

Analysis of field distributions provide critical insight on the mechanics underlying plasmonic coupling. Key parameters of the field at resonance (RI = 1.38) are summarized in Table 2. Constructive interference between the two plasmonic interfaces is responsible for the improved field confinement in the π-configuration, which preserves enough penetration depth for analyte interaction while producing concentrated areas of strong electromagnetic energy density. The D-shaped sensor shows a slightly higher penetration depth, d_p compared to the π-configuration sensor. A larger d_p allows a sensor to detect changes deeper into the analyte, which might be beneficial for some applications. However, a higher sensitivity sensor, which is driven by a more concentrated field, is often a more critical performance metric for detecting small changes in RI at the sensor's surface. This is a deliberate design choice that optimizes the sensor for applications requiring high precision and a low detection limit, rather than for bulk sensing.

Table 2. Electric field characteristics at peak wavelengths.

Parameter	π-Configuration	D-Shaped	Enhancement Factor
Peak |E| (V/m)	140	100	1.40×
Field Penetration Depth (nm)	243	247	0.98×
Coupling Efficiency (%)	84.5	67.5	1.25×

3.3. Sensors Performance Metric Comparison

For the π-configuration and D-shaped optical fibre sensors, various performance metrics such as the FWHM, figure of merit (FOM), and confinement loss are compared at analyte RI of 1.38.

As indicated in Table 3, a thorough performance evaluation was carried out utilizing several quality indicators. Due to the combined effect of reduced resonance width and increased sensitivity, the π-configuration performs better on all measures, including the figure of merit (FOM). This implies that the π-configuration SPR-based optical fibre sensor has a better ability to accurately determine the true value of the refractive index or concentration of an analyte. The π-configuration increases confinement loss while decreasing resonance FWHM, which is a significant finding. This design improves the coupling efficiency from the core mode to the surface plasmon, which explains the rationale for confinement loss.

In contrast, the FWHM is determined by the propagation loss of the plasmonic mode itself. The smaller FWHM suggests that the π-configuration enables a plasmonic mode with reduced inherent dissipation, resulting in a sharper resonance and greater sensing resolution, despite the larger power transfer from the core. The sharp resonance peak as seen in Figure 2b shows a smaller FWHM, implying an improved SNR. Hence, the signal from the analyte is strong and clearly distinguishable from background noise. This proposed sensor can resolve smaller differences in the RI, making it suitable for detecting minute molecular binding events or low concentration of analytes in a sample.

Table 3. Comparison of sensors performance metrics (RI = 1.38).

Metric	π-Configuration (Ag)	D-Shaped (Ag)	Enhancement
FWHM (nm)	36	38	0.95×
FOM (RIU^{-1})	94.29	39.47	2.4×
Confinement Loss (dB/cm)	38.5	8.2	4.7×

Figure 7a,b shows the graph of confinement loss against the incident light wavelength for the π-configuration and D-shaped SPR sensors, respectively.

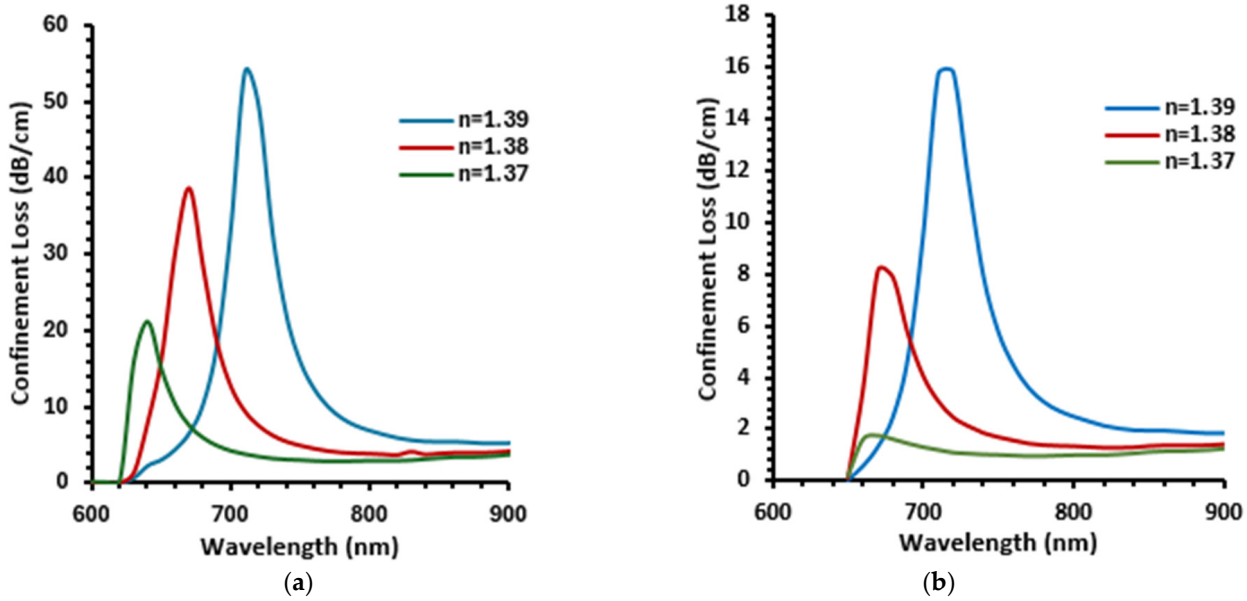


Figure 7. Confinement loss spectra for (**a**) π-configuration; (**b**) D-shaped sensor.

Confinement loss in this design context is the amount of light that leaks out of the core of the optical fibre and is absorbed by the metallic thin film. The π-configuration shows a higher confinement loss compared to the D-shaped sensor. This means that more of the core-guided light is successfully transferred to the SPP mode. The energy from the leaked core excites the SPPs which are highly confined to the metal surface. This causes an increase in the evanescent field extending into the analyte. The higher the confinement loss, the more intense the evanescent field. A comparison of this design with existing designs from literature is presented in Table 4.

Table 4. Comparison of the performance of this π-configuration Ag optical fibre SPR sensor with other optical sensors published in the literature.

Ref.	Sensor Configuration	Sensing Material	RI Range	Wavelength Sensitivity (nm/RIU)	Resolution (RIU)
[42]	D-SPR Fibre	Gold	1.35–1.43	925	-
[43]	Dual core D-shaped PCF	Silver	1.30–1.33	2066	-
[44]	D-shaped Fibre	Gold	1.37–1.39	2500	-
[9]	D-shaped SPR PCF	Silver	1.33–1.40	3128	-
[20]	D-shaped SPR	Silver	1.37–1.38	1500	8.13×10^{-6}
	This work (π-configuration)	Silver	1.37–1.38	3300	8×10^{-6}

Environmental robustness is an important consideration in the practical deployment of any optical sensor. While the proposed π-configuration demonstrates significant sensitivity enhancement in a controlled refractive index window, its practical deployment must account for environmental interferents, particularly temperature fluctuations. The thermo-optic effect of the silica fibre, metal layers, and aqueous analyte collectively induce a temperature-dependent resonance shift, which is a fundamental challenge for any label-free optical biosensor [45]. A detailed quantification of this temperature sensitivity, requiring coupled Multiphysics modelling of the constituent materials' thermophysical properties, extends beyond the scope of this theoretical investigation focused on geometric innovation. This critical engineering analysis, alongside experimental validation and compensation strategies, will be addressed in our subsequent work aimed at developing a field-ready prototype.

Furthermore, humidity changes can disrupt the evanescent field by altering the effective cladding index or, more severely, by causing condensation on the plasmonic surface, concealing the unique sensor response. While air pressure has a relatively minimal effect due to the pressure-dependent refractive index of the ambient medium, its impact may become significant in precise atmospheric sensors or controlled industrial situations [46].

4. Conclusions

A thorough theoretical and numerical analysis of the novel π-configuration SPR-based optical fibre sensor has shown its potential for ultra-sensitive biomolecular detection. By using coupled-mode theoretical modelling and rigorous finite element analysis, we have demonstrated that the dual-interface plasmonic coupling mechanism results in remarkable sensitivity enhancements, especially in the critical low refractive index range (1.37–1.38) where conventional single-interface designs exhibit limited performance. When compared to conventional D-shaped designs, the π-configuration's exceptional capacity to increase the evanescent field–analyte interaction volume while maintaining strong field confinement leads to a 120% increase in sensitivity for silver-coated sensors (3300 nm/RIU vs. 1500 nm/RIU). The maximum field norm for the π-configuration sensor is approximately 1.4 times greater than the maximum observed for the D-shaped SPR sensor at an analyte RI of 1.38. At the two metal–dielectric interfaces, constructive interference between counter-propagating surface plasmon polaritons produces a steep dispersion relation that amplifies wavelength shifts in response to minute changes in refractive index. This is the underlying basis for this enhancement.

Silver's outstanding plasmonic properties, which include low optical losses ($\mathrm{Im}(\varepsilon) < 3.5$) and a high negative real permittivity ($\mathrm{Re}(\varepsilon) < -40$) in the visible-to-near-

infrared spectrum makes it an excellent choice for this dual-interface architecture, according to material optimization studies. The sensor outperforms existing state-of-the-art designs while still being practically feasible to fabricate. Its performance measures, such as its remarkable figure of merit (94.29 RIU^{-1}) and detection accuracy (0.94), demonstrate this. By using critical coupling theory, which operates close to ideal conditions ($\kappa/\alpha \approx 1$) for maximum energy transfer between the guided mode and hybridized plasmonic modes, the nonlinear response characteristics—particularly the disproportionate sensitivity enhancement at lower refractive indices—have been explained. This fundamental knowledge of the dynamics of dual interface coupling creates new opportunities for designing plasmonic sensors with specific sensitivity profiles. The key novelty of this research is the development of a symmetric, π-shaped fibre plasmonic sensor, which significantly improves on the traditional D-shaped design. This design offers a significant advantage by allowing the use of two opposing sensing regions on the polished surfaces, which provide a concentrated and uniform electric field that penetrates the fibre core with significantly better efficiency than the fringe field from a single-sided sensing region. This enhanced field confinement directly translates into increased sensitivity and resonance sharpness. Furthermore, the symmetric geometry places the core between the sensing regions, decreasing performance variability caused by lateral misalignment during manufacturing and resulting in a more robust and manufacturable sensor platform than the alignment-sensitive single-sided D-shaped fibre. The π-configuration sensor enables inherent multi-analyte detection by functionalizing each flat surface with a different bioreceptor, allowing for simultaneous, label-free sensing of distinct targets from a single sample—a functionality that is extremely difficult to implement reliably in a D-shaped sensor.

With immediate uses in point-of-care testing, environmental monitoring, and early illness diagnosis, the π-configuration SPR-based fibre optic sensor is a breakthrough in optical biosensing technology. It is a flexible platform for next-generation biosensors due to its ability to multiplex detection by selective functionalization of the dual sensing interfaces and compatibility with conventional optical fibre production procedures. To improve the environmental stability of silver, future research will concentrate on the experimental implementation of the design, biofunctionalization procedure improvement, and protective coating exploration. The study's findings could potentially transform the field of label-free molecular detection by pushing sensitivity limits beyond existing capabilities while preserving reliable, field-deployable sensor architectures. These principles could also be applied to other waveguide geometries and plasmonic materials.

Author Contributions: Conceptualization, J.E., R.P. and S.K.; methodology, J.E. and R.P.; software, J.E., R.P. and S.K.; investigation, J.E., R.P. and S.K.; data curation, J.E. and R.P.; writing—original draft preparation, J.E.; writing—review and editing, R.P. and S.K.; visualization, J.E., R.P. and S.K.; supervision, R.P. and S.K. All authors have read and agreed to the published version of the manuscript.

Funding: This research received no external funding.

Data Availability Statement: The data supporting the findings of this study are available from the corresponding author upon reasonable request.

Acknowledgments: I would like to acknowledge the support provided by the School of Engineering, Robert Gordon University, in this research study.

Conflicts of Interest: The authors declare no conflicts of interest.

References

1. Soler, M.; Huertas, C.S.; Lechuga, L.M. Label-free plasmonic biosensors for point-of-care diagnostics: A review. *Expert Rev. Mol. Diagn.* **2019**, *19*, 71–81. [CrossRef]
2. Berini, P. Long-range surface plasmon polaritons. *Adv. Opt. Photonics* **2009**, *1*, 484–588. [CrossRef]
3. Capelli, D.; Scognamiglio, V.; Montanari, R. Surface plasmon resonance technology: Recent advances, applications and experimental cases. *TrAC Trends Anal. Chem.* **2023**, *163*, 117079. [CrossRef]
4. Tokel, O.; Inci, F.; Demirci, U. Advances in plasmonic technologies for point of care applications. *Chem. Rev.* **2014**, *114*, 5728–5752. [CrossRef]
5. Gupta, B.D.; Shrivastav, A.M.; Usha, S.P. Surface plasmon resonance-based fiber optic sensors utilizing molecular imprinting. *Sensors* **2016**, *16*, 1381. [CrossRef]
6. Liu, Y.; Li, S.; Chen, H.; Li, J.; Zhang, W. Surface plasmon resonance-induced high sensitivity refractive index sensor with adjustable measurement range based on an evanescent field-enhanced D-shaped five-hole photonic crystal fiber. *J. Phys. D* **2020**, *53*, 115107. [CrossRef]
7. Xiong, Y.; Xu, F. Multifunctional integration on optical fiber tips: Challenges and opportunities. *Adv. Photonics* **2020**, *2*, 64001. [CrossRef]
8. Yu, X.; Zhang, S.; Olivo, M.; Li, N. Micro-and nano-fiber probes for optical sensing, imaging, and stimulation in biomedical applications. *Photonics Res.* **2020**, *8*, 1703–1724. [CrossRef]
9. Bai, G.; Yin, Z.; Li, S.; Jing, X.; Chen, Q.; Zhang, M.; Shao, P. Enhancement of SPR effect and sensing characteristics in D-shaped polished grapefruit microstructured optical fiber with silver film. *Opt. Commun.* **2023**, *530*, 129204. [CrossRef]
10. Liu, L.; Liu, Z.; Zhang, Y.; Liu, S. Side-polished D-type fiber SPR sensor for RI sensing with temperature compensation. *IEEE Sens. J.* **2021**, *21*, 16621–16628. [CrossRef]
11. Homola, J.; Piliarik, M. Surface Plasmon Resonance (SPR) Sensors. In *Surface Plasmon Resonance Based Sensors*; Springer: Berlin/Heidelberg, Germany, 2006.
12. Homola, J. Surface plasmon resonance sensors for detection of chemical and biological species. *Chem. Rev.* **2008**, *108*, 462–493. [CrossRef]
13. Wang, J.; Lu, X.; Mi, C.; Yin, Q.; Lv, J.; Yang, L.; Liu, W.; Yi, Z.; Liu, Q.; Chu, P.K.; et al. Ultra-high sensitivity photonic crystal fiber sensor based on dispersion turning point sensitization of surface plasmonic polariton modes for low RI liquid detection. *Opt. Express* **2024**, *32*, 32895–32908. [CrossRef] [PubMed]
14. Naik, G.V.; Shalaev, V.M.; Boltasseva, A. Alternative plasmonic materials: Beyond gold and silver. *Adv. Mater.* **2013**, *25*, 3264–3294. [CrossRef]
15. Kumari, A.; Vyas, V.; Kumar, S. Synthesis, characterization, and applications of gold nanoparticles in development of plasmonic optical fiber-based sensors. *Nanotechnology* **2022**, *34*, 42001. [CrossRef] [PubMed]
16. McMillan, J.A. Higher Oxidation States of Silver. *Chem. Rev.* **1962**, *62*, 65–80. [CrossRef]
17. Bhavsar, K.; Prabhu, R.; Pollard, P. Ultrasensitive graphene coated SPR sensor for biosensing applications. In *Optical Sensors 2015*; SPIE: Bellingham, WA, USA, 2015.
18. Sharma, A.K.; Mohr, G.J. On the performance of surface plasmon resonance based fibre optic sensor with different bimetallic nanoparticle alloy combinations. *J. Phys. D* **2008**, *41*, 55106. [CrossRef]
19. Wang, L.; Hasanzadeh Kafshgari, M.; Meunier, M. Optical properties and applications of plasmonic-metal nanoparticles. *Adv. Funct. Mater.* **2020**, *30*, 2005400. [CrossRef]
20. Ehiabhili, J.; Prabhu, R.; Kannan, S. Highly sensitive D-SPR sensors with optimized metallic thin films for bio-analyte detection. *Photonics* **2024**, *11*, 764. [CrossRef]
21. Liu, L.; Deng, S.; Zheng, J.; Yuan, L.; Deng, H.; Teng, C. An enhanced plastic optical fiber-based surface plasmon resonance sensor with a double-sided polished structure. *Sensors* **2021**, *21*, 1516. [CrossRef]
22. Lalanne, P.; Yan, W.; Vynck, K.; Sauvan, C.; Hugonin, J. Light interaction with photonic and plasmonic resonances. *Laser Photonics Rev.* **2018**, *12*, 1700113. [CrossRef]
23. Alabastri, A.; Tuccio, S.; Giugni, A.; Toma, A.; Liberale, C.; Das, G.; De Angelis, F.; Di Fabrizio, E.; Zaccaria, R.P. Molding of plasmonic resonances in metallic nanostructures: Dependence of the non-linear electric permittivity on system size and temperature. *Materials* **2013**, *6*, 4879–4910. [CrossRef]
24. Ghosh, S.K.; Pal, T. Interparticle coupling effect on the surface plasmon resonance of gold nanoparticles: From theory to applications. *Chem. Rev.* **2007**, *107*, 4797–4862. [CrossRef]
25. Luka, G.; Ahmadi, A.; Najjaran, H.; Alocilja, E.; DeRosa, M.; Wolthers, K.; Malki, A.; Aziz, H.; Althani, A.; Hoorfar, M. Microfluidics integrated biosensors: A leading technology towards lab-on-a-chip and sensing applications. *Sensors* **2015**, *15*, 30011–30031. [CrossRef]
26. Bona, G.; Germann, R.; Offrein, B.J. SiON high-refractive-index waveguide and planar lightwave circuits. *IBM J. Res. Dev.* **2003**, *47*, 239–249. [CrossRef]

27. Lin, Z.; Wu, G.; Zhao, L.; Lai, K.W.C.; Lai, W. Carbon nanomaterial-based biosensors: A review of design and applications. *IEEE Nanotechnol. Mag.* **2019**, *13*, 4–14. [CrossRef]
28. Jilani, A.; Abdel-Wahab, M.S.; Hammad, A.H. Advance deposition techniques for thin film and coating. In *Modern Technologies for Creating the Thin-Film Systems and Coatings*; IntechOpen: London, UK, 2017; Volume 2, pp. 137–149.
29. Verhagen, E. *Subwavelength Light Confinement with Surface Plasmon Polaritons*; Utrecht University: Utrecht, The Netherlands, 2009.
30. Ivanov, O.V.; Nikitov, S.A.; Gulyaev, Y.V. Cladding modes of optical fibers: Properties and applications. *Phys.-Uspekhi* **2006**, *49*, 167. [CrossRef]
31. Mulchan, N.M.; Rodriguez, M.; O'sHea, K.; Darici, Y. Application of a high-resolution SPR technique for monitoring real-time metal/dielectric interactions. *Sens. Actuators B Chem.* **2003**, *88*, 132–137. [CrossRef]
32. Rioux, D.; Vallières, S.; Besner, S.; Muñoz, P.; Mazur, E.; Meunier, M. An analytic model for the dielectric function of Au, Ag, and their alloys. *Adv. Opt. Mater.* **2014**, *2*, 176–182. [CrossRef]
33. Kirsch, A.; Hettlich, F. The mathematical theory of time-harmonic Maxwell's equations. *Appl. Math. Sci.* **2015**, *190*, 20.
34. Rafi, H.N.; Kaysir, M.R.; Islam, M.J. Air-hole attributed performance of photonic crystal fiber-based SPR sensors. *Sens. Bio-Sens. Res.* **2020**, *29*, 100364. [CrossRef]
35. Yang, H.; Wang, G.; Lu, Y.; Yao, J. Highly sensitive refractive index sensor based on SPR with silver and titanium dioxide coating. *Opt. Quant. Electron.* **2021**, *53*, 341. [CrossRef]
36. Hoseinian, M.S.; Bolorizadeh, M.A. Design and simulation of a highly sensitive SPR optical fiber sensor. *Photonic Sens.* **2019**, *9*, 33–42. [CrossRef]
37. Vig, J.R.; Walls, F.L. A review of sensor sensitivity and stability. In Proceedings of the 2000 IEEE/EIA International Frequency Control Symposium and Exhibition (Cat. No. 00CH37052), Kansas, MO, USA, 9 June 2000.
38. Kadhim, R.A.; Yuan, L.; Xu, H.; Wu, J.; Wang, Z. Highly sensitive D-shaped optical fiber surface plasmon resonance refractive index sensor based on Ag-α-Fe_2O_3 grating. *IEEE Sens. J.* **2020**, *20*, 9816–9824. [CrossRef]
39. Worthing, P.T.; Barnes, W.L. Efficient coupling of surface plasmon polaritons to radiation using a bi-grating. *Appl. Phys. Lett.* **2001**, *79*, 3035–3037. [CrossRef]
40. Bharadwaj, R.; Mukherji, S.; Mukherji, S. Probing the localized surface plasmon field of a gold nanoparticle-based fibre optic biosensor. *Plasmonics* **2016**, *11*, 753–761. [CrossRef]
41. Sebastian, M.T.; Ubic, R.; Jantunen, H. Low-loss dielectric ceramic materials and their properties. *Int. Mater. Rev.* **2015**, *60*, 392–412. [CrossRef]
42. Ying, Y.; Wang, J.; Hu, N.; Xu, K.; Sun, L.; Si, G. Determination of refractive index using surface plasmon resonance (SPR) and rigorous coupled wave analysis (RCWA) with a D-shaped optical fiber and a nano-gold grating. *Instrum. Sci. Technol.* **2020**, *48*, 376–385. [CrossRef]
43. Li, Y.; Chen, C.; Liu, X.; Gong, A.; Shen, T. Performance comparison and analysis of D-type single and dual-core PCF-SPR sensors. *Phys. Scr.* **2023**, *98*, 95025. [CrossRef]
44. Pathak, A.K.; Singh, V.K.; Ghosh, S.; Rahman, B.M.A. Investigation of a SPR based refractive index sensor using a single mode fiber with a large D shaped microfluidic channel. *OSA Contin.* **2019**, *2*, 3008–3018. [CrossRef]
45. Kosmalska-Olańska, A.; Olszewski, J.; Masek, A. A brief review of optical polymers in material engineering. *Express Polym. Lett.* **2024**, *18*, 1291–1326. [CrossRef]
46. Kim, Y.; Celliers, P.M.; Eggert, J.H.; Lazicki, A.; Millot, M. Interferometric measurements of refractive index and dispersion at high pressure. *Sci. Rep.* **2021**, *11*, 5610. [CrossRef] [PubMed]

Disclaimer/Publisher's Note: The statements, opinions and data contained in all publications are solely those of the individual author(s) and contributor(s) and not of MDPI and/or the editor(s). MDPI and/or the editor(s) disclaim responsibility for any injury to people or property resulting from any ideas, methods, instructions or products referred to in the content.